

# 100 nm period gratings produced by lithographically induced self-construction

Xinya Lei, Lin Wu, Paru Deshpande, Zhaoning Yu, Wei Wu, Haixiong Ge and Stephen Y Chou

NanoStructure Laboratory, Department of Electrical Engineering, Princeton University, Princeton, NJ 08544, USA

Received 11 November 2002, in final form 17 March 2003

Published 13 May 2003

Online at [stacks.iop.org/Nano/14/786](http://stacks.iop.org/Nano/14/786)

## Abstract

In this paper we report a technique that allows a fast replication of sub-100 nm scale patterns in a thin polymer film on a substrate from a patterned mask. Using the new pattern transfer technique, we fabricated 100 nm period polymer gratings with a 50 nm linewidth above a Si substrate as an example to demonstrate its capability of producing sub-100 nm nanostructures with direct industrial applications. In our technique, a mask with protruding patterns is used to induce similar pattern formation in the molten polymer film through an electrohydrodynamic instability process. A solid positive replica of the mask is obtained by cooling the polymer below its glass transition temperature. The mask is removed afterwards for the next fabrication procedure. The polymer structures formed can be used either directly as functional devices or as etching masks for further lithography processes. The mechanism that leads to the instability and subsequent pattern formation in the polymer layer is explained. Several important physical parameters that control the whole instability process are also identified. Our theory and experiments show that the pattern transfer technique developed here is well suited for the fabrication of sub-100 nm surface patterns in thin polymer films.

(Some figures in this article are in colour only in the electronic version)

## 1. Introduction

Conventional photolithography has been widely used in the fabrication of microelectronic and other micrometre scale devices. It has the advantages of allowing arbitrary pattern design, high throughput, and low cost. But the wavelength of the light imposes a fundamental limit on the photolithography technique, which makes it difficult and expensive to photolithographically make devices with a feature size smaller than 100 nm. Other nanolithography techniques such as electron beam lithography (EBL) and x-ray lithography (XRL) are capable of achieving sub-10 nm feature size, but EBL is limited by its serial processing nature and XRL has the disadvantage of high cost. Self-assembly techniques provide alternative methods with low-cost and high-throughput advantages in nanofabrication. But due to the fact that the nucleation happens randomly during the self-assembly process, the resulting self-assembled patterns are

multi-domained and suffer from large numbers of defects. It is very difficult to achieve self-assembled uniform patterns over large areas [1]. The self-assembly technique also has limited selection of pattern geometry. The new lithographically induced self-construction (LISC) technique not only inherits all the advantages of the self-assembly technique but also introduces a strong guidance mechanism into the self-assembly process [2]. As a result, the LISC patterns can be arbitrarily designed in advance, and the final patterns are well organized and can be well controlled.

However, the feature size of the patterns created by LISC in previous work was on the micrometre scale [2]. In this paper we improve the LISC technique to make it suitable for the fast construction of sub-micrometre patterns in thin polymer films. To demonstrate its capability of producing sub-100 nm nanostructures with direct industrial applications, we present the detailed fabrication steps for making 100 nm period gratings with a 50 nm linewidth by LISC. This sub-100 nm

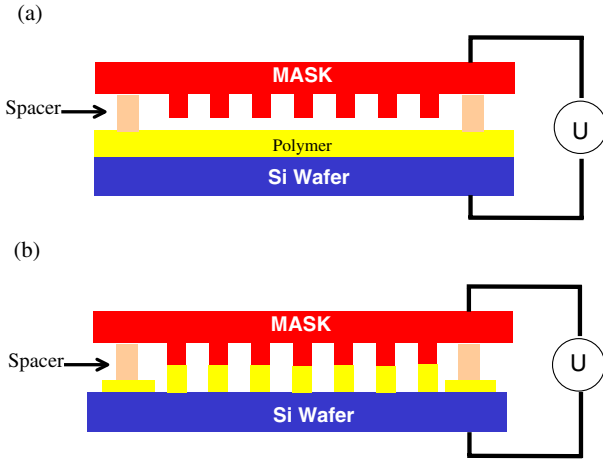


**Figure 1.** A diagram of the LISC experimental set-up. (a) A grating mask was placed a certain distance above the polymer film and an external electric field was applied; (b) the assembly was heated up to 140 °C and the polymer film self-constructed into a pattern which has a lateral dimension identical to that of the mask.

feature size, which is an order of magnitude smaller than that of the previous LISC work, was achieved by appropriate scaling of the initial polymer film thickness, the gap between the substrate and the mask, and the electric field, based on a scaling theory.

## 2. Experiment

The experimental set-up is shown in figure 1. A thin polymer film was spin-coated onto a silicon wafer. Then, a silicon mask with pre-fabricated protruding patterns was placed a certain distance above the wafer, leaving a thin air gap in between them. Spacers were used to maintain the spacing between the polymer film and the mask protrusions. The spacers also electrically isolated the substrate and the mask. The assembly was then heated above the glass transition temperature ( $T_g$ ) of the polymer. A DC voltage was applied between the substrate and the mask. After its formation, the polymer feature was annealed for about 4 min before it was immobilized by cooling it to room temperature. Subsequently the mask (top electrode) was mechanically removed. The final morphology of the polymer films was investigated by atomic force microscopy (AFM) and by scanning electron microscopy (SEM).

After the grating patterns on the silicon mask were fabricated using the interference lithography and reactive ion etching [3], the sample was covered by a 1 mm thick metal foil punched with a hole array. Each hole had a diameter of 0.5 mm and the separation between the holes was 2 mm. Then, the whole sample was put into an electron beam evaporator. SiO<sub>2</sub> was grown on the mask surface within the holes, while the unexposed previously fabricated gratings were protected. The final SiO<sub>2</sub> spacers were formed after the removal of the metal foil. The height of the spacers was measured by a DekTak profilometer. The mask was rinsed with acetone before it was coated with a surfactant with low surface energy to facilitate the mask–substrate separation after the LISC.

In our experiments, polymethyl methacrylate (PMMA) was used as the LISC formation material. PMMA solution

(3 wt%) with a polymer molecular weight of 2000 was spin-coated onto a silicon wafer using a Karl Suss spinner. The PMMA film was baked for 3 min at 80 °C to dry out the solvent. The thickness of the PMMA film was measured with an ellipsometer (Rudolph/Auto EL). The film thickness can be controlled in the range of 70–100 nm. For example, a 70 nm thick uniform film was obtained by using the spinner in open hood mode at a spin speed of 3000 rpm. The air gap between the PMMA film and the mask protrusions was controlled by the spacers and was in the range of 40–100 nm. The mask and the substrate (with spin-coated polymer) were firmly pressed together by applying a pressure as large as 1 atm to the mask. The mask–polymer–substrate assembly was heated up from room temperature to 140 °C. A DC voltage (5–10 V) was externally applied during the heating cycle.

## 3. Theoretical explanation and scaling

In LISC, the pattern formation in the polymer films is a result of a hydrodynamic instability occurring at the air–polymer interface. The instability is driven by the electrostatic force exerted on the free charges or dipoles accumulated at the interface [4–6].

In the following analysis, we adopt a two-dimensional and one-layer liquid motion model (see figure 2). The melting polymer flow is assumed to be a highly viscous incompressible Newtonian flow with a low Reynolds number. The air motion is ignored. The flow is a pressure-driven Poiseuille flow [7]. The governing equation is the Stokes equation. After taking into account the spacing in the film thickness direction being much smaller than the length scale in the horizontal direction, one obtains the following lubrication equations:

$$0 = -\frac{\partial p}{\partial x} + \mu \frac{\partial^2 u}{\partial z^2}, \quad (1a)$$

$$0 = -\frac{\partial p}{\partial z}, \quad (1b)$$

where  $p$  is the pressure,  $u$  is the polymer velocity in the  $x$ -direction (horizontal),  $\mu$  is the dynamic viscosity of the polymer. Equation (1a) can be integrated twice to give the velocity distribution in the  $z$ -direction subject to a nonslip boundary condition at the lower polymer–solid interface ( $z = 0$ ) and a disappearance-of-shear-stress condition at the polymer–air interface ( $z = h$ ). Subsequently, the horizontal volume flow rate of the polymer across the film thickness is obtained as  $q_x = \int_0^h u \, dz = -\frac{1}{3\mu} \frac{\partial p}{\partial x} h^3$ , where  $h(t, x)$  is the polymer film thickness ( $t$  is the time). Finally, mass balance gives the governing equation for the thickness of the polymer layer:

$$\frac{\partial h}{\partial t} + \frac{\partial q_x}{\partial x} = 0. \quad (2)$$

The pressure  $p$  across the film thickness is a constant (equation (1b)), which is determined by the normal stress balance at the polymer–air interface ( $z = h$ ):  $p = p_0 - \sigma h_{xx} / (1 + h_x^2)^{3/2} + p_e + p_{dis}$ , where  $p_0$  is the ambient air pressure,  $\sigma$  is the surface tension coefficient of the polymer.  $h_x$  and  $h_{xx}$  are the first- and second-order derivatives of  $h$  with respect to  $x$ , respectively.  $p_e$  is an electrostatic pressure exerted on the interface by the interaction

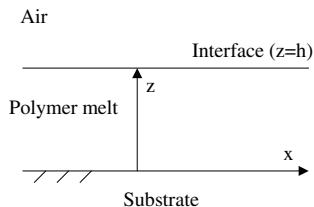


**Figure 2.** The coordinate system used for the theoretical analysis.

of the electrical field with the polarization charges at the interface. Here we simply adopt the following model:  $p_e = -\epsilon_0\epsilon_p(\epsilon_p - 1)U^2/[\epsilon_p d - (\epsilon_p - 1)h]^2$ , where  $\epsilon_0$  and  $\epsilon_p$  are the dielectric constants of the air and the polymer, respectively [4].  $U$  is the voltage applied between the mask and the substrate.  $d$  is the distance between the top mask and the lower substrate. The disjoining pressure  $p_{dis}$  caused by the intermolecular forces exerted on the polymer film can be modelled as  $p_{dis} = A_2/h^2 - A_3/h^3$ , where  $A_2$  is a constant of the order of  $10^{-12}$  N and  $A_3$  is of the order of  $10^{-19}$  N m [8].

The dimensionless governing equation for the interface thickness can be written as

$$\frac{\partial H}{\partial t} + \frac{\partial}{\partial X} \left( H^3 \frac{\partial P}{\partial X} \right) = 0, \quad (3)$$

where  $H$  is the dimensionless film thickness normalized by the initial film thickness  $h_0$ .  $X$  is the dimensionless horizontal coordinate normalized by the width of the mask pattern  $L$ .  $t$  is the dimensionless time normalized by a timescale  $t^* \sim 3\mu L^2/U^2\epsilon_0\epsilon_p(\epsilon_p - 1)$ .  $P = \alpha H_{XX}/(1 + R_l H_X^2)^{3/2} + 1/(\epsilon_p D - (\epsilon_p - 1)H)^2 - \beta_2/H^2 + \beta_3/H^3$  is the normalized pressure, where  $\alpha = \sigma h_0^3/U^2 L^2 \epsilon_0 \epsilon_p (\epsilon_p - 1)$  is a dimensionless parameter, which is the ratio between the surface tension force and the electrostatic force.  $R_l = h_0/L$  is a length scale ratio.  $D = d/h_0 > 1$  is the dimensionless gap between the mask and the substrate.  $\beta_2 = A_2/U^2\epsilon_0\epsilon_p(\epsilon_p - 1)$  and  $\beta_3 = A_3/h_0 U^2 \epsilon_0 \epsilon_p (\epsilon_p - 1)$  are ratios between the dispersion forces and the electrostatic force.

The following normal mode is adopted for  $H$  to transform equation (3) into a linear ordinary differential equation in a standard linear instability analysis:

$$H = \tilde{H} \exp(ik(x - ct)), \quad (4)$$

where  $\tilde{H}$  is the amplitude function,  $k$  is the wavenumber, and  $c = c_r + ic_i$  is the modified growth rate, which is a complex number. According to the definition of the normal mode used (equation (4)), a positive  $c_i$  represents an unstable system, and a negative  $c_i$  represents a stable system. After substituting equation (4) into (3), we obtain  $c_r = 0$  and  $c_i = -\alpha k^4 + (2(\epsilon_p - 1)/(\epsilon_p D - \epsilon_p + 1)^3 + 2\beta_2 - 3\beta_3)k^2$ , where  $\epsilon_p$  and  $D$  are greater than 1. In a typical LISC experimental set-up, the film thickness is around 100 nm, which corresponds to negligibly small  $\beta_2$  and  $\beta_3$ . Thus we have  $2(\epsilon_p - 1)/(\epsilon_p D - \epsilon_p + 1)^3 + 2\beta_2 - 3\beta_3 > 0$ , and we can always find positive  $c_i$  if the wavenumber  $k$  is small enough. As a result, the system is always unstable subject to infinitesimal disturbance. From the above relationship between  $c_i$  and  $k$ , we can find the most unstable wavelength of the system:

$$\lambda_m = 2\pi L \sqrt{\frac{2\alpha(\epsilon_p D - \epsilon_p + 1)^3}{2(\epsilon_p - 1) + (2\beta_2 - 3\beta_3)(\epsilon_p D - \epsilon_p + 1)^3}}. \quad (5)$$

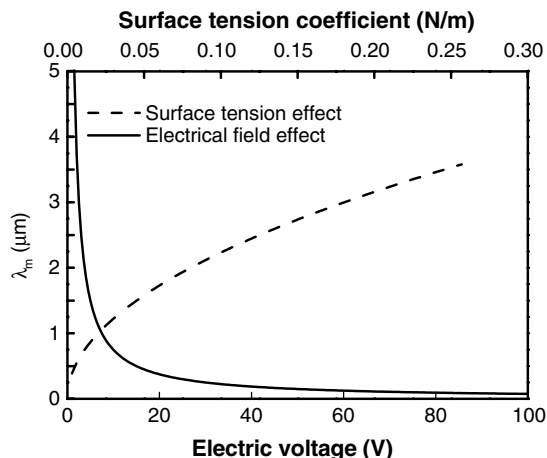


**Figure 3.** Plots of feature size versus the surface tension coefficient and the electric voltage according to the scaling theory (equation (5)). The dashed curve corresponds to a fixed 5 V external electric voltage and a fixed space ratio  $D = 1.571$ , which were the parameters used in the following experiment. The solid curve corresponds to a space ratio  $D = 1.571$  and a fixed surface tension coefficient of 2 K PMMA ( $0.031 \text{ N m}^{-1}$ ).

The numerical simulation using equation (3) shows that if the linewidth of the gratings on the mask is smaller than the most unstable wavelength given by equation (5), LISC patterns with lateral dimension identical to that of the mask would form in the polymer film [9].

For a particular structure with feature size  $L$ ,  $L \leq \lambda_m$  is a sufficient condition for forming the corresponding LISC structure. Figure 3 plots  $\lambda_m$  as a function of the externally applied voltage  $U$  and the polymer's surface tension coefficient  $\sigma$ . As plotted in figure 3, the theory suggests that a smaller feature size can be achieved by a smaller initial polymer film thickness, a smaller ratio between the mask–substrate separation and the initial film thickness, a smaller surface tension coefficient, and a stronger electrical field. When the initial film thickness is well below 100 nm, the intermolecular forces have to be included. Otherwise their effect can be ignored.

#### 4. Results and discussion

In the first case, we fabricated the 200 nm PMMA gratings with a 100 nm linewidth. The LISC patterns were characterized by using an atomic force microscope and a scanning electron microscope. Figure 4(a) shows the SEM image of a 200 nm period grating mask with a 100 nm linewidth used in the fabrication. The thickness of the initially flat PMMA film was 100 nm. The height of the spacers on the mask was 200 nm. As a result, the gap between the mask and the polymer was 100 nm. The externally applied voltage was 10 V, which resulted in an external electric field strength of  $5 \times 10^5 \text{ V cm}^{-1}$ . Figure 4(b) shows the SEM image of the PMMA grating patterns formed. The grating patterns were regular and uniform over a large area. The AFM image (figure 4(c)) of the polymer structure formed reveals that the height of the PMMA grating lines is 35 nm. The period of the polymer gratings is 200 nm and their linewidth is 100 nm; these values are identical to those for the mask.

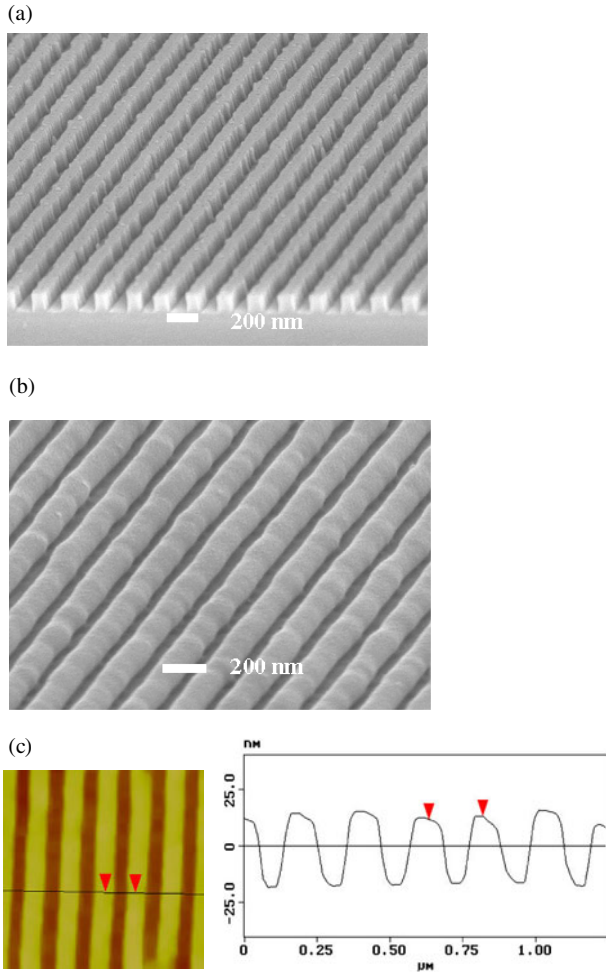


**Figure 4.** (a) The SEM image of the silicon mask with a 200 nm period grating and a 100 nm linewidth. (b) The SEM image of the PMMA gratings with a 200 nm period and a 100 nm linewidth. (c) The AFM image of the PMMA gratings with a 200 nm period and a 100 nm linewidth.

Next, we fabricated 100 nm period PMMA gratings with a 50 nm linewidth. Figure 5(a) is the SEM image of the mask. The thickness of the initially flat PMMA film was 70 nm. The height of the spacers was 110 nm, and the gap was 40 nm. During the heating cycle, a 5 V voltage was externally applied to the sample. The external electric field strength was  $4.5 \times 10^5 \text{ V cm}^{-1}$ . Figure 5(b) shows the SEM image of the PMMA gratings formed. The replicated gratings were regular and uniform over a large area. The AFM image (figure 5(c)) reveals that the polymer gratings have a height of 10 nm and they have a 100 nm period with a linewidth of 50 nm, identical to the values for the mask.

The aspect ratio (height/width) of the gratings is 0.35 for the 200 nm period PMMA gratings and 0.2 for the 100 nm PMMA gratings. The round cross-sectional shape of the PMMA gratings in both the 200 and the 100 nm period cases is assumed to be induced by the minimization of the liquid polymer surface energy during the annealing process. Although the detailed morphology might change with certain experimental parameters, such as the thickness of the polymer film and the air gap spacing, we found that the LISC process works over a wide range of these parameters.

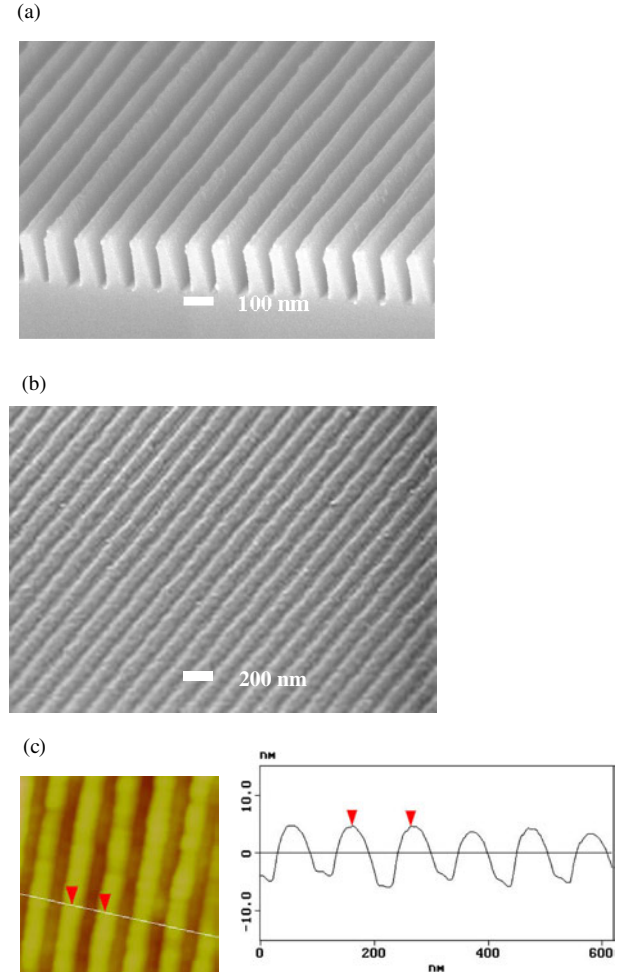


**Figure 5.** (a) The SEM image of the silicon mask with a grating pattern with a 100 nm period and a 50 nm linewidth. (b) The SEM image of the PMMA gratings with a 100 nm period and a 50 nm linewidth. (c) The AFM image of the PMMA gratings with a 100 nm period and a 100 nm linewidth.

At a temperature of 140 °C, the surface tension coefficient  $\sigma$  of the 2 K PMMA is about  $0.031 \text{ N m}^{-1}$  [10]. The dielectric constant of the PMMA is 3.6. When we substituted all the experimental parameters into equation (5), we found that for both cases the unstable wavelengths  $\lambda_m$  are much larger than the linewidths of the grating on the mask. For the first case, the theory predicts  $\lambda_m$  to be  $2.351 \mu\text{m}$ . For the second case,  $\lambda_m$  is  $1.243 \mu\text{m}$ . Both predicted values of  $\lambda_m$  are one order of magnitude larger than the grating linewidth. We obtained a LISC mesa underneath the mask as explained in section 3 and in figure 3.

## 5. Conclusions

In summary, we have developed a LISC technique for achieving 50 nm feature size by appropriately choosing the experimental parameters according to a scaling theory. With further improvements, patterns with a feature size smaller than 10 nm and an aspect ratio larger than 1 should be achievable. LISC fabrication combines the advantages of conventional lithography with those of conventional self-assembly. LISC is well suited for forming sub-100 nm size structures, because

if the mask feature size is smaller than the most unstable disturbance wavelength of the system, which is normally micrometre sized, a LISC mesa will form. This approach to patterning nanostructures without using resists, exposures, developers, and etchings may find application in the fabrication of electronic, optoelectronic, and biological devices.

### Acknowledgment

This work was partially supported by DARPA.

### References

- [1] Xia Y, Rogers J A, Paul K E and Whitesides G M 1999 *Chem. Rev.* **99** 1823
- [2] Chou S Y, Zhuang L and Guo L 1999 *Appl. Phys. Lett.* **75** 1004
- [3] Yu Z, Wei W, Chen L and Chou S Y 2001 *J. Vac. Sci. Technol. B* **19** 2816
- [4] Schaffer E, Thurn-Albrecht T, Russell T P and Steiner U 2001 *Europhys. Lett.* **53** 518
- [5] Suo Z and Liang J 2001 *Appl. Phys. Lett.* **78** 3971
- [6] Pease L F and Russel W B 2002 *J. Non-Newton. Fluid Mech.* **102** 233
- [7] Panton R L 1996 *Incompressible Flow* 2nd edn (New York: Wiley)
- [8] Teletzke G F, Davis H T and Scriven L E 1988 *Revue Phys. Appl.* **23** 989
- [9] Wu L and Chou S Y 2003 *Appl. Phys. Lett.* to be published
- [10] Brandrup J and Immergut E H 1989 *Polymer Handbook* 3rd edn (New York: Wiley)